

LETTER • OPEN ACCESS

## Indicators of upcoming electric breakdown in a pyroelectric accelerator

To cite this article: Pavel Karataev *et al* 2022 *Appl. Phys. Express* **15** 066001

View the [article online](#) for updates and enhancements.

### You may also like

- [Thermally induced atmospheric pressure gas discharges using pyroelectric crystals](#)  
Michael J Johnson, John Linczer and David B Go
- [Wind-driven pyroelectric energy harvesting device](#)  
Mengying Xie, Daniel Zabek, Chris Bowen et al.
- [Enhanced Pyroelectric Coefficient in Ferroelectric Lead Zirconium Titanate Thick Films for Thermal Energy Harvesting Applications](#)  
Vandana, Reema Gupta, R. P. Tandon et al.



## Indicators of upcoming electric breakdown in a pyroelectric accelerator

Pavel Karataev<sup>1\*</sup>, Andrei Oleinik<sup>2\*</sup> , Kirill Fedorov<sup>1</sup>, Artemiy Klenin<sup>2</sup>, Alexander Kubankin<sup>2,3</sup>, and Alexander Shchagin<sup>2,4</sup>

<sup>1</sup>John Adams Institute at Royal Holloway, University of London, Egham, TW20 0EX, United Kingdom

<sup>2</sup>Laboratory of Radiation Physics, Belgorod National Research University, Belgorod, Russia

<sup>3</sup>Lebedev Physical Institute, Moscow, Russia

<sup>4</sup>Kharkov Institute of Physics and Technology, Kharkov, Ukraine

\*E-mail: [Pavel.Karataev@rhul.ac.uk](mailto:Pavel.Karataev@rhul.ac.uk); [oleynik\\_a@bsu.edu.ru](mailto:oleynik_a@bsu.edu.ru)

Received April 4, 2022; revised April 20, 2022; accepted April 28, 2022; published online May 17, 2022

This paper describes indicators that can be used to monitor the operating mode of a pyroelectric accelerator. It is shown that the ratio of the characteristic X-ray emission lines from the target and the vacuum chamber walls is very sensitive to the state of the accelerator. Also, the peak to total count rate ratio in the electron spectrum exhibits similar properties. These parameters change sharply ahead of the electric breakdown and are very sensitive to the residual gas pressure level. Monitoring these indicators during the accelerator operation provides a fine tool aiding the implementation of pyroelectric technology for stable and reliable charged particle generation and acceleration.

© 2022 The Author(s). Published on behalf of The Japan Society of Applied Physics by IOP Publishing Ltd

The development of high-brightness and high-power electron and X-ray sources<sup>1)</sup> has always been accompanied by the development of compact, robust, and energy-efficient X-ray and electron generators.<sup>2)</sup> The application range of these devices goes far beyond the use in a laboratory or a specialized institution. In some cases, a direct high voltage applied to the cathode needs to be avoided. As is well known, temperature change (pyroelectric effect),<sup>3)</sup> mechanical compression/expansion (piezoelectric effect),<sup>4)</sup> as well as friction (triboelectric effect)<sup>5)</sup> can initiate the generation of high electric field potential due to polarization of certain dielectric materials. It has been repeatedly demonstrated that pyroelectric materials (usually single crystals of lithium niobate or tantalate) driven by a temperature change can be used to generate and accelerate electrons<sup>6–13)</sup> and ions.<sup>14–16)</sup> The concept of the pyroelectric accelerator has been introduced by several groups.<sup>17–19)</sup> It has also been used to generate X-rays,<sup>20–34)</sup> neutrons,<sup>35–37)</sup> and to control charged particle beams.<sup>38)</sup>

Even though there is a commercially available pyroelectric X-ray generator,<sup>39)</sup> pyroelectric accelerators have not yet widespread applications due to the weak reproducibility of the particle fluxes.<sup>20,33)</sup> The main reason is the electric breakdowns<sup>22,27,37)</sup> in the gap between the pyroelectric crystal and the target, which can occur due to a disbalance between the positive and negative polarity phases during thermal cycling. Crystal impurities and roughness of its surface<sup>32)</sup> are negative factors, leading to unpredictable electric breakdowns and unstable accelerator operation. The aim of this research is to develop a technique to predict the upcoming breakdown during the operation of the pyroelectric accelerator and to further counteract its action. We describe the parameters of the X-ray and electron spectra, which can be used as indicators of either the upcoming electric breakdown or a stable operating mode. A way to monitor the pyroelectric accelerator operation online and predict the upcoming electric breakdown at the negative polarity phase (electron emission from the crystal surface) has been proposed and analysed.

The pyroelectric accelerator has been assembled inside a vacuum chamber. The geometry of the experiment is shown

in Fig. 1. A single crystal of lithium tantalate (LiTaO<sub>3</sub>, LT) with a rectangular shape has been chosen to drive the accelerator. The crystal size is 20 × 20 × 10(z) mm. The temperature of the LT has been changed using a Peltier element. The heat from the opposite side of the Peltier element was extracted by an aluminium heatsink. A brass target of 0.5 mm thick and 50 × 70 mm area was placed at a distance of 10 mm from the top surface of the crystal. A hole of 0.3 mm diameter was made in the target coaxially with the crystal. Therefore, the target also played the role of the electron flux collimator. The electron flux spectrum was recorded by an Ortec-CR-012-025-100 surface-barrier particle detector, located behind the target coaxially with the hole at a distance of 30 mm away from it. The X-ray spectrum was recorded by an Amptek Cd-Te X-123 spectrometer, mounted on a side flange of the vacuum chamber at a distance of about 750 mm from the vertical axis through the centre of the crystal, the hole, and the particle detector. The X-ray detector is 5 mm higher vertically than the top surface of the crystal, which makes it possible to observe X-ray emissions both from the target and the crystal, as well as from the vacuum chamber wall. In addition, the electron current through the pyroelectric accelerator was measured using the Keithley 6485 picoammeter connected in series with the bottom surface of the crystal and the target, as shown in Fig. 1.

Figure 2 presents the X-ray and electron spectra. The X-ray spectrum [Fig. 2(a)] contains lines of copper (Cu K $\alpha$  = 8.048 keV) and zinc (Zn K $\alpha$  = 8.639 keV), which referred to the target material. In addition, there are lines of iron (Fe K $\alpha$  = 6.404 keV) and chromium (Cr K $\alpha$  = 5.415 keV) corresponding to the vacuum chamber material. The electron irradiation of the chamber walls leads to X-ray fluorescence. In addition, secondary fluorescence is produced by the X-rays emitted from the target.<sup>26,29)</sup> Figures 2(b) and 2(c) present the electron spectra recorded at the start of the observation and at the maximum intensity. The structure of the spectra is visually quite different. The peak and its harmonics<sup>8,11,14)</sup> appear at the start and closer to the end of the negative polarity phase. The presence of harmonics is associated with the pile-up effect during the high intensity of monoenergetic electron flux, i.e., several electrons



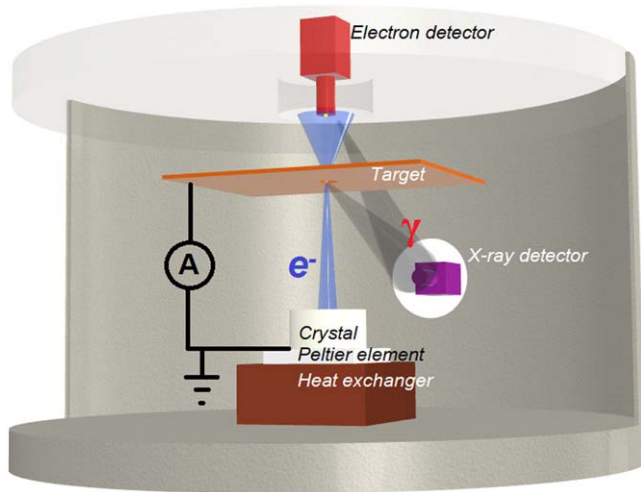


**Fig. 1.** (Color online) Scheme for measurement of the X-ray and electron fluxes generated by the pyroelectric accelerator based on a LiTaO<sub>3</sub> single crystal (shown in beige), the temperature of which is changed using a Peltier element (shown in white). The electron flux is indicated in blue, and the X-ray flow is in grey. An electric circuit for measurement of the electron current is shown by the black line.

might be detected simultaneously providing double, triple, quadruple, etc. electron energy in the spectrum. The energy of the main peak does not exceed 20 keV. An increase in the electric potential leads to both an increase in the total electron intensity and a weaker manifestation of the peak, as it is shown in Fig. 2(c). But in this case, the peak energy rises to the level of 45–50 keV, which satisfactorily agrees with the endpoint energy of the X-ray spectrum.

An analysis of the spectra dynamics reveals several peculiarities that can be used to monitor the pyroelectric accelerator performance. Two indicators have been clearly identified. The first one is the ratio of the integral numbers of photons in the characteristic copper line from the target and in the iron line from the vacuum chamber wall (Cu/Fe line ratio). The secondary electrons make a significant contribution to the fluorescence of the Cu line, therefore, Cu/Fe ratio is related to the contribution of secondary electrons to the total electron flux. The second indicator is the ratio between the number of electrons in the peak (and its harmonics) and the total number of electrons in the spectrum (peak/total ratio). The electrons in the peak correspond to the primary emission from the crystal; accordingly, a decrease in the ratio means an increase in the secondary electrons. Figure 3 shows the typical behaviour of both indicators in stable operation mode, i.e., no interruption of the particle generation is observed [Fig. 3(a)] and when electric breakdown appears [Fig. 3(b)]. We note that the electron current pattern with an avalanche is reproduced in both cases, however, the behaviour of the indicators is different. The Cu/Fe line ratio steadily increases during stable operation, thereby, the contribution of the target line to the spectrum increases. At the same time, the contribution of the peaks to the total electron spectrum decreases till the electron current reaches its maximum. During the fall of the electron current level, the peak/total counts ration grows again. This pattern is reproduced every time at the stable negative polarity operation of the pyroelectric accelerator. This behaviour can be explained by the contribution of the secondary electrons kicked off

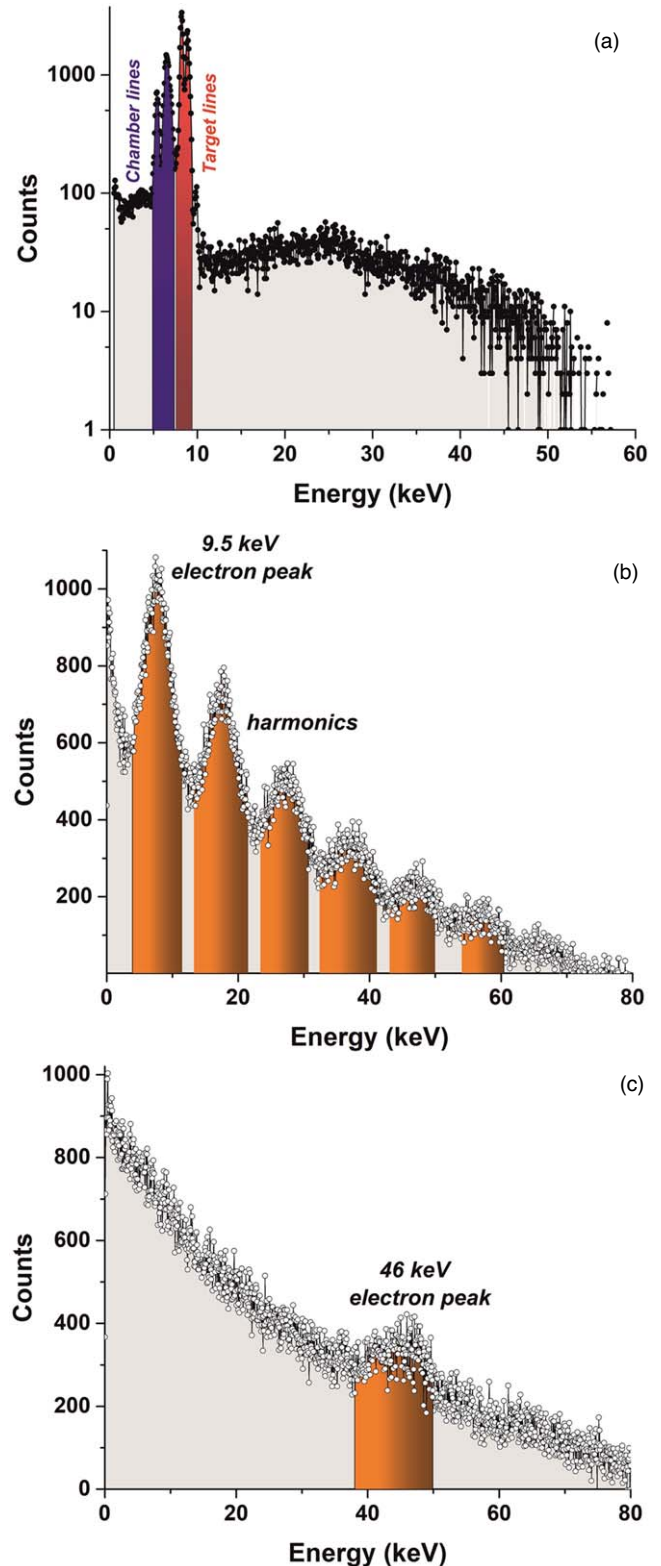


**Fig. 2.** (Color online) (a) An X-ray spectrum obtained during the operation of the pyroelectric accelerator at the negative polarity phase. The red colour corresponds to the characteristic lines emitted from the target; the blue colour corresponds to the photons emitted from the vacuum chamber walls. (b) and (c) Electron spectra obtained at the beginning of the observation and at the maximum intensity of the electron beam, respectively. The electron peak and its harmonics are highlighted in orange colour.

from the target and accelerated back to it. In addition, the diverging electron flux leads to an increase in the target area irradiated by the electrons<sup>40)</sup> and, as a result, changes the observation geometry of the X-ray detector.

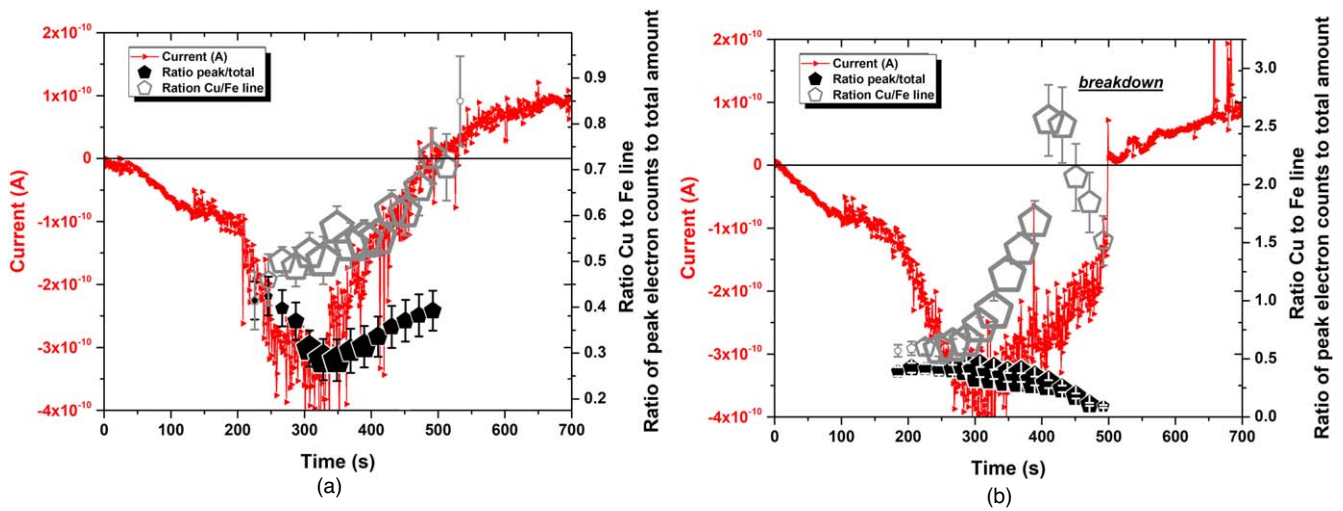


**Fig. 3.** (Color online) Behaviour of the Cu/Fe ratio (white pentagon) and the peak/total ratio (black pentagon) at the negative polarity of the pyroelectric accelerator operation. The electron current is shown in red colour. (a) Stable operation. (b) The manifestation of the electric breakdown.

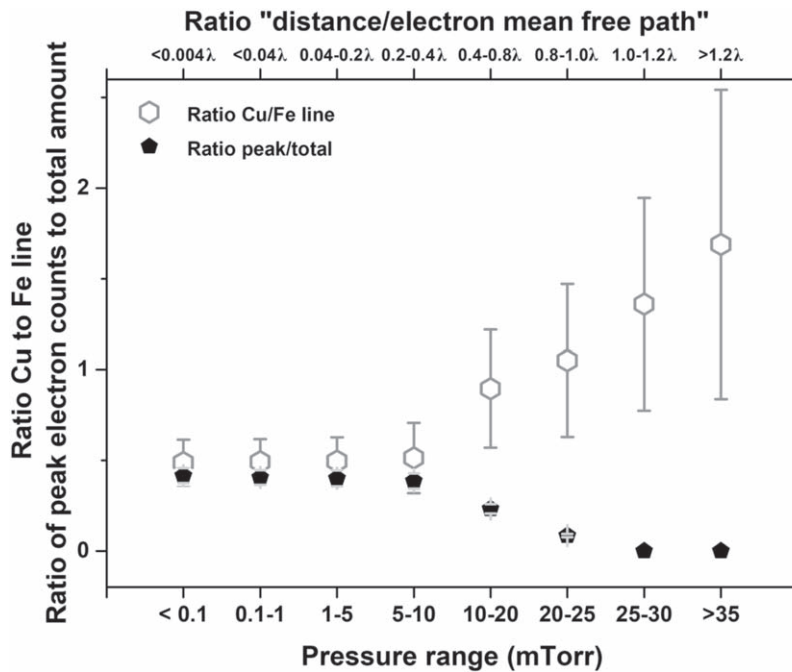


**Fig. 4.** (Color online) Dependence of the average value of the Cu/Fe ratio (white pentagon) and the peak/total ratio (black pentagon) on the residual gas pressure. Only stable operation cycles (i.e., no interruption of the particle flow) are used to accumulate statistics.

However, in the case of electric breakdown, the behaviour of these indicators greatly changes. The contribution of the Cu line increases much faster than in the case of stable operation. Before the breakdown (approximately 20–60 s ahead), the Cu/Fe ratio starts to fall gradually meaning the transition to a pre-breakdown state. The peak/total ratio also drops gradually ahead of the electric breakdown. The pre-breakdown state can be explained by an increase in the number of secondary electrons emitted from the target. However, the energy of the secondary electrons is insufficient to generate X-rays. At the same time, the secondary emission gradually increases with a decrease in the energy of the electrons<sup>41)</sup> moving back to the target. Nevertheless, the mechanism of electric breakdown requires careful analysis.

Note, that the probability of electric breakdown very strongly depends on the residual gas pressure. We have

noticed that the behaviour of the indicators depends on the pressure as well. The average value of each indicator as a function of the pressure is shown in Fig. 4. It should be noted that the fraction of stable operation cycles becomes smaller with an increase in the pressure, which also drives the increase of the error for the Cu/Fe ratio. It can be seen that the stability continues up to 10 mTorr. Further increase in the pressure leads to the change in the average value of the indicators, signaling a more unstable operating mode. The results in Fig. 4 refer to a distance between the crystal and the target of 10 mm. However, the change in the distance can shift the threshold between the stable and unstable regions. The top horizontal axis in Fig. 4 shows the ratio of the distance between the crystal and the target to the mean free path of an electron ( $\lambda \approx 250 \text{ mm/mTorr}$  for nitrogen, according to the kinetic theory of gases<sup>42)</sup>) at the

corresponding pressure range. The stable operation of the accelerator lasts up to approximately the level when the electron path between the crystal and the target reaches half the mean free path. Further increase in this ratio causes the generation of additional low energy electrons due to impact ionization. These electrons contribute to the development of instabilities.

We noticed that the indicator values strongly depend on the distance between the crystal and the target and other geometric parameters. However, the behaviour of indicators shown in Fig. 3 remains unchanged for the same experimental geometry of a pyroelectric accelerator. By monitoring the indicators one may anticipate the breakdown. The next step would be to develop a mechanism to avoid the breakdown, e.g., to prevent it from happening. That would be a real breakthrough for the pyroelectric accelerator operation principles. The most promising mechanism is the fine regulation of the temperature change law in order to slow down the charge induction on the surface of the pyroelectric material.<sup>31)</sup> Due to the fact that the breakdown approaches rather slowly, one may adjust the target-to-detector distance. Theoretically, it is possible to stabilise the pyroelectric accelerator by pressure regulation,<sup>33)</sup> but such a mechanism is difficult to implement in a vacuum-sealed device.

In conclusion, we should say that we have demonstrated the indicators of stable operation of the pyroelectric accelerator. The indicators signal the upcoming electric breakdown. The quantitative values of the indicators come from the ratio of the components of the X-ray and electron spectra. We have demonstrated their typical behaviour in a stable regime and just before the electric breakdown that stops the operation of the accelerator. The analysis shows that the residual gas pressure has a strong influence on stability. Above a certain value of the residual gas pressure together with the geometric parameters, the accelerator operation is unstable. The monitoring of the indicators makes the operation of the pyroelectric accelerator predictable and shows the real way to the realization of stable practical devices.

**Acknowledgements** The research was supported by a grant from the Russian Science Foundation (Project No. 21-72-00006).

**ORCID iDs** Andrei Oleinik  <https://orcid.org/0000-0002-1455-4341>

- 1) H. Wiedemann, *Introduction to Accelerator Physics*. (Springer, Cham, 2015) 1029.
- 2) A. Gorecka-Drzazga, *J. MEMS* **26**, 295 (2017).
- 3) J. D. Brownridge, *Trends in Electro-Optics Research* (Nova Science Publishers, New York, 2005) 37.
- 4) O. Ivashchuk, A. Shchagin, A. Kubankin, I. Nikulin, A. Oleinik, V. Miroshnik, and V. Volkov, *Sci. Rep.* **8**, 16488 (2018).
- 5) J. Hird, C. Camara, and S. Putterman, *Appl. Phys. Lett.* **98**, 133501 (2011).
- 6) G. Rosenman and D. Shur, *J. Appl. Phys.* **88**, 6109 (2000).
- 7) J. D. Brownridge and S. M. Shafroth, *Appl. Phys. Lett.* **79**, 3364 (2001).
- 8) J. D. Brownridge, S. M. Shafroth, D. W. Trott, B. R. Stoner, and W. M. Hooke, *Appl. Phys. Lett.* **78**, 1158 (2001).
- 9) S. Fukao, Y. Ito, and S. Yoshikado, *Key Eng. Mater.* **23**, 248 (2003).
- 10) N. Kukhtarev, T. Kukhtareva, M. Bayssie, J. Wang, and J. D. Brownridge, *J. Appl. Phys.* **96**, 6794 (2004).
- 11) V. I. Nagaychenko, V. A. Voronko, V. V. Sotnikov, V. V. Sidorenko, P. S. Kizim, A. M. Yegorov, and A. V. Shchagin, *Prob. At. Sci. Tech.* **5**, 72 (2008).
- 12) S. Imashuku, A. Imanishi, and J. Kawai, *Rev. Sci. Instrum.* **84**, 073111 (2012).
- 13) S. Mohtashami, H. Afarideh, F. Abbasi Davani, and R. Ghaderi, *JINST* **16**, P10017 (2021).
- 14) J. A. Geuther and Y. Danon, *J. Appl. Phys.* **97**, 074109 (2005).
- 15) E. L. Neidholdt and J. L. Beauchamp, *J. Amer. Soc. Mass Spectr.* **20**, 2093 (2009).
- 16) V. I. Nagaychenko, V. S. Miroshnik, A. M. Yegorov, and A. V. Shchagin, *Prob. At. Sci. Tech.* **2**, 34 (2010).
- 17) T. Z. Fullem and Y. Danon, *J. Appl. Phys.* **106**, 074101 (2009).
- 18) A. V. Shchagin, V. S. Miroshnik, V. I. Volkov, and A. N. Oleinik, *Appl. Phys. Lett.* **107**, 233505 (2015).
- 19) R. Ghaderi and F. A. Davani, *Appl. Phys. Lett.* **106**, 042906 (2015).
- 20) J. D. Brownridge, *Appl. Phys. Lett.* **85**, 1298 (2004).
- 21) S. Fukao, Y. Nakanishi, Y. Guan, Y. Sato, Y. Ito, and S. Yoshikado, *Key Eng. Mater.* **24**, 22 (2004).
- 22) V. I. Nagaychenko, V. M. Sanin, A. M. Yegorov, and A. V. Shchagin, *Prob. At. Sci. Tech.* **2**, 214 (2004).
- 23) J. A. Geuther and Y. Danon, *J. Appl. Phys.* **97**, 104916 (2005).
- 24) S. Fukao, Y. Nakanishi, J. Kondo, Y. Ito, and S. Yoshikado, *Key Eng. Mater.* **301**, 205 (2006).
- 25) S. Imashuku, A. Imanishi, and J. Kawai, *Anal. Chem.* **83**, 8363 (2011).
- 26) J. Kawai, H. Ishiib, and H. Idac, *X-ray Spectrom.* **41**, 216 (2012).
- 27) S. Imashuku and J. Kawai, *Rev. Sci. Instrum.* **83**, 016106 (2012).
- 28) Y. Alivov, M. Klopfer, and S. Molloy, *Appl. Phys. Lett.* **102**, 143106 (2013).
- 29) O. O. Ivashchuk, A. S. Kubankin, A. N. Oleinik, and A. V. Shchagin, *J. Synchron. Investig.* **8**, 16 (2016).
- 30) A. S. Chepurinov, O. O. Ivashchuk, E. P. Kitsyuk, A. A. Klenin, A. S. Kubankin, R. M. Nazhmudinov, A. N. Oleinik, A. A. Pavlov, and A. V. Shchagin, *JINST* **12**, P11002 (2017).
- 31) A. S. Kubankin, A. S. Chepurinov, O. O. Ivashchuk, V. Y. U. Ionidi, I. A. Kishin, A. A. Klenin, A. N. Oleinik, and A. V. Shchagin, *AIP Adv.* **8**, 035207 (2018).
- 32) O. O. Ivashchuk, A. A. Klenin, A. S. Kubankin, A. N. Oleinik, and A. V. Shchagin, *J. Nano-Electron. Phys.* **10**, 06014 (2018).
- 33) K. Hanamoto, T. Kataoka, and K. Yamaoka, *Appl. Radiat. Isot.* **135**, 40 (2018).
- 34) M. Wilke, K. Harnisch, W. Knapp, M. Ecke, and T. Halle, *J. Vac. Sci. Tech. B* **37**, 011203 (2019).
- 35) B. Naranjo, J. Gimzewski, and S. Putterman, *Nature* **434**, 1115 (2005).
- 36) J. Geuther, Y. Danon, and F. Saglime, *Phys. Rev. Lett.* **96**, 54803 (2006).
- 37) W. Tornow, S. M. Shafroth, and J. D. Brownridge, *J. App. Phys.* **104**, 034905 (2008).
- 38) A. N. Oleinik, A. S. Kubankin, R. M. Nazhmudinov, K. A. Vokhmyanina, A. V. Shchagin, and P. V. Karataev, *JINST* **11**, P08007 (2016).
- 39) Pyroelectric X-ray source COOL-X, Amptek URL: <http://amptek.com/pdf/coolx.pdf>.
- 40) R. Ghaderi and F. A. Davani, *Appl. Phys. Lett.* **105**, 232906 (2014).
- 41) M. Azzolini, M. Angelucci, R. Cimino, R. Larciprete, N. M. Pugno, S. Taioli, and M. Dapor, *J. Phys. Condens. Matter* **31**, 055901 (2019).
- 42) H. B. Wahlin, *Phys. Rev.* **23**, 169 (1924).